Competing structural ordering tendencies in Heusler-type alloys with high Curie temperatures: $Fe_2CoGa_{1-x}Zn_x$ studied by first-principles calculations

Antje Dannenberg,[1] Mario Siewert,[1] Markus E. Gruner,[1] Manfred Wuttig,[2] and Peter Entel[1]
[1]*Faculty of Physics and Center for Nanointegration, CeNIDE, University of Duisburg-Essen, 47048 Duisburg, Germany*
[2]*Department of Materials Science and Engineering, University of Maryland, College Park, Maryland 20742-2115, USA*
(Received 14 October 2010; published 20 December 2010)

The influence of Zn substitution on the structural, magnetic, and electronic properties and lattice vibrations of ferromagnetic $Fe_2CoGa_{1-x}Zn_x$ alloys in the conventional X_2YZ and inverse $(XY)XZ$ Heusler structures is investigated, by means of *ab initio* and Monte Carlo calculations, which predict strong ferromagnetic coupling and high Curie temperatures between 770 and 925 K. In the Ga-rich systems the inverse Heusler structure is energetically favored but no indication for a structural instability is found in contrast to Fe-Co-Ga-Zn alloys in the conventional Heusler structure. The origin of the remarkably strong preference of the cubic $(c/a=1)$ inverse phase is believed to originate from the bcc-like environment of the two inequivalent Fe atoms and their stronger hybridization with the Co states compared to the conventional structure. In the quaternary compounds, $Fe_2CoGa_{1-x}Zn_x$, substitution of Ga by Zn reduces the energetic preference of the inverse structure caused by weakening of the Co-Fe hybridization. Simultaneously, Zn leads to higher magnetic moments and Curie temperatures because of localization effects. In addition, since Zn weakens the miscibility of the alloys, we propose that the composition of $Fe_2CoGa_{1-x}Zn_x$ alloys has to be carefully chosen in order to yield an interesting future ferromagnetic shape-memory alloy system.

DOI: 10.1103/PhysRevB.82.214421 PACS number(s): 71.15.Mb, 71.15.Nc, 75.20.En, 63.20.dk

I. INTRODUCTION

Smart materials as, for instance, ferromagnetic shape-memory alloys (FSMAs) are subject of intensive research because of their potential use for actuator and sensor applications. Prototype Ni_2MnGa, although showing a large strain effect of 10% in a magnetic field of less than 1 T,[1] is not perfectly suitable for magnetomechanical devices since the martensitic transition occurs at a too low temperature (with martensite start temperature $M_S \approx 200$ K for the near-stoichiometric samples and $M_S \approx 350$ K for the technologically relevant $Ni_{50}Mn_{30}Ga_{20}$) and because the material is rather brittle. Thus, higher M_S has only been achieved for off-stoichiometric samples by substituting, for example, Mn for Ga. This has the disadvantage of lowering the Curie temperature T_C and the magnetic shape-memory effect (MSME) because of antiferromagnetic correlations induced by the additional Mn atoms. Therefore, new material combinations with improved elastic properties and higher Curie and martensite transformation temperatures are required. So far, several new candidates for FSMAs have been proposed, including the Ni-Mn-(Al,Ga,In,Sn,Sb) series,[2,3] Co-Ni-(Al,Ga),[4–11] Ni-Fe-Al,[12] and Cu-Mn-(Al,Ga).[13,14]

Here, we propose to start from well-known binary cubic alloy systems which already show martensitic tendencies. Our aim is to predict ferromagnetic X_2YZ Heusler alloys with improved properties in which X and Y are transition-metal elements of the binary systems and Z=Ga or Zn is the element which introduces (s,p)-valence electrons and helps to stabilize the Heusler structure. The element Zn can substitute Al, Ga, and Sn in the X_2YZ Heusler compounds. Promising binary systems are, e.g., Fe_3Ga,[15–17] Co_3Fe,[18] CoGa,[19] CoZn,[20,21] FeZn,[20–22] and FeGa.[23,24] Up to now zinc was not considered very often, partially because of its too high vapor pressure. But Zn is known to be beneficial for alloying in ternary, nonmagnetic Ni- or Cu-based shape-memory alloys such as Cu-Zn-Al.[25–27] Furthermore, FeZn alloys with a Zn concentration of 20–40 % show a huge magnetostriction[22] as, for example, Fe_3Ga.[16]

In off-stoichiometric Ni-Mn-Ga alloys the martensite start temperature M_S shows a linear dependence on the valence-electron concentration per atom, e/a. M_S may considerably be enhanced by increasing the e/a ratio.[28] Detailed investigations of the electronic density of states (DOS) show that providing additional valence electrons, for example, by replacing Ga by Mn in Ni_2MnGa, shifts the Fermi level E_F to higher energies away from the pseudogaplike region in the minority-spin channel in a rigid bandlike manner.[29]

Although in detail the change in chemical bonding and magnetic properties with e/a is more complicated, this shows that e/a may be considered as the parameter which governs M_S and the magnetic correlations. Therefore, systems with a different e/a ratio than stoichiometric Ni_2MnGa $(e/a=7.5)$ may be considered as promising candidates with higher martensitic transformation temperatures. Unfortunately, for the Ni-Mn-Ga system it is difficult to increase simultaneously the Curie temperature T_C because excess Mn atoms may occupy the Ga sites leading to nearest-neighbor Mn-Mn atoms which interact antiferromagnetically.[29]

The prediction of systems having higher M_S and T_C which are not based on Ni-Mn becomes hampered by the fact that different distributions of atoms on the lattice sites which can be conceived as four interpenetrating fcc lattices may result in new phases having lower energies as it is the case for the so-called inverse Heusler structure of Fe_2CoGa shown in Fig. 1(b).

A remarkable combinatorial study of 810 conventional and inverse Heusler alloys on the basis of first-principles total-energy calculations was performed by Gilleßen and Dronskowski[30,31] in which the thermochemical stability of

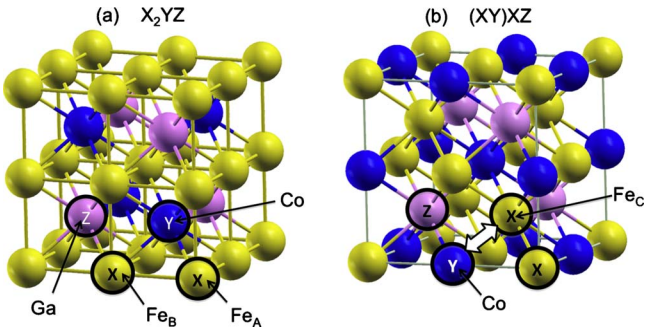

FIG. 1. (Color online) (a) The cubic unit cell of Fe_2CoGa in the conventional Heusler structure (denoted by X_2YZ) in which iron atoms Fe_A and Fe_B (light spheres) occupy the X sites and Co (dark spheres) and Ga atoms (medium gray spheres) share one cubic sublattice and occupy Y and Z sites, respectively. (b) Inverse Heusler [denoted by $(XY)XZ$] structure in which the Co and one Fe atom exchange their sites. One of the two X sites is now occupied by Co. The interchanged Fe atom is marked as Fe_C. The remaining half of the Fe atoms stays at their original sites.

the conventional X_2YZ structure is compared with the related inverse $(XY)XZ$ Heusler structure. The brackets in $(XY)XZ$ indicate that the atoms X and Y now occupy the X_2 lattice sites while X and Z occupy the Y- and Z-lattice sites of the conventional X_2YZ structure. They find 27 stable inverse phases. Despite this large effort, their calculations do not include material combinations being of interest for future FSMAs or combinations which we discuss in this paper, where Zn partially substitutes the element Z. Furthermore they do not provide Curie temperatures, mixing energies, and phonon-dispersion relations, which are of primary interest for FSMA.

In order to fill this gap it is worthwhile to consider new combinations of X, Y, and Z elements avoiding the elements Ni (leading to brittle Heusler alloys) and Mn (causing antiferromagnetic correlations). We limit the discussion to two ternary stoichiometric systems, Fe_2CoGa and Fe_2CoZn, and related nonstoichiometric quaternary $Fe_2CoGa_{1-x}Zn_x$ alloys. In order to deal with aspects of structural stability of the conventional versus the inverse structure, we consider also mixing energies and phonon-dispersion relations of both type of structures of Fe_2CoGa and Fe_2CoZn compounds and $Fe_2CoGa_{1-x}Zn_x$ alloys.

Early Mössbauer studies of Co_2FeGa and Fe_2CoGa revealed atomic-site preferences showing that Co_2FeGa has a well-ordered, conventional Heusler structure, while in Fe_2CoGa the Co atoms occupy one of the two fcc Fe sublattices,[32] compare Fig. 1(b). Concerning the structural ordering a general trend was observed, transition-metal atoms to the left of Fe prefer to occupy the Y site while those on the right of Fe preferentially go to the X sublattice.[32] In order to account for these site preferences and resulting structures, we have considered the two different types of Heusler structures shown in Fig. 1. The conventional Heusler structure X_2YZ and the inverse Heusler structure $(XY)XZ$. In the latter case the X atoms become nearest neighbors.

We use density-functional theory for the investigation of their structural, magnetic, electronic, and dynamical characteristics. For the structural investigation including the calculation of the force constants and for the evaluation of mixing energies we employed the Vienna *ab initio* simulation package (VASP).[33] For the calculation of magnetic-exchange parameters we used the spin-polarized Korringa-Kohn-Rostoker (KKR) code by Hubert Ebert from LMU Munich.[34,35] The Curie temperatures were evaluated by inserting the magnetic-exchange parameters into the Heisenberg model and performing Monte Carlo simulations.

As was pointed out before, numerous studies in search for better suited magnetic shape-memory materials with im-

TABLE I. Calculated equilibrium parameters of cubic and tetragonal ternary Fe_2CoGa and Fe_2CoZn and quaternary $Fe_2CoGa_{1-x}Zn_x$ systems in the conventional X_2YZ and in the inverse $(XY)XZ$ Heusler structure. Valence-electron concentration e/a, structural stability, equilibrium lattice constant a_0 for the cubic $(c/a=1)$ phase, local and absolute energy minima at different tetragonal distortions c/a, total magnetic moment M per formula unit and Curie temperature T_C in kelvin of the $c/a>1$ phases, energy difference in the X_2YZ structure between the cubic phase at $c/a=1$ and the absolute energy minimum at $c/a>1$, $\Delta E_{c/a}$, and energy difference between the conventional X_2YZ and inverse $(XY)XZ$ ordered structure, ΔE_{order}, in milli-electron-volt per atom. "/" means no second minimum in the $E(c/a)$ curve. The calculation shows that the equilibrium volume of the cubic phase, $V_0=a_0^3$, does practically not change when the system undergoes a tetragonal distortion $(c/a\neq 1)$, i.e., $a^2c\simeq a_0^3$.

System	e/a	Structure	a_0 (Å)	c/a		M (μ_B/f.u.)	T_C	$\Delta E_{c/a}$	ΔE_{order}	E_{mix}
Conventional										
Fe_2CoGa	7	Stable in $L1_0$	5.774	0.88	1.46	6.08	770	55	44	−463
$Fe_2CoGa_{0.75}Zn_{0.25}$	6.9375	Stable in $L1_0$	5.779	0.91	1.44	6.22	802	53.5	31	−333
$Fe_2CoGa_{0.25}Zn_{0.75}$	6.8125	Stable in $L1_0$	5.780	0.9	1.42	6.51	896	49	6	−721
Fe_2CoZn	6.75	Unstable	5.782	0.92	1.40	6.64	925	47	−9	51
Inverse										
(FeCo)FeGa	7	Stable at $c/a=1$	5.736	1.0	/	5.29	780	/		−642
(FeCo)$FeGa_{0.75}Zn_{0.25}$	6.9375	Stable at $c/a=1$	5.744	1.0	/	5.58	768	/		−458
(FeCo)$FeGa_{0.75}Zn_{0.75}$	6.8125	Stable at $c/a=1$	5.748	1.0	/	5.58	830	/		−328
(FeCo)FeZn	6.75	Unstable	5.750	1.0	1.36	5.95	850	−11		135

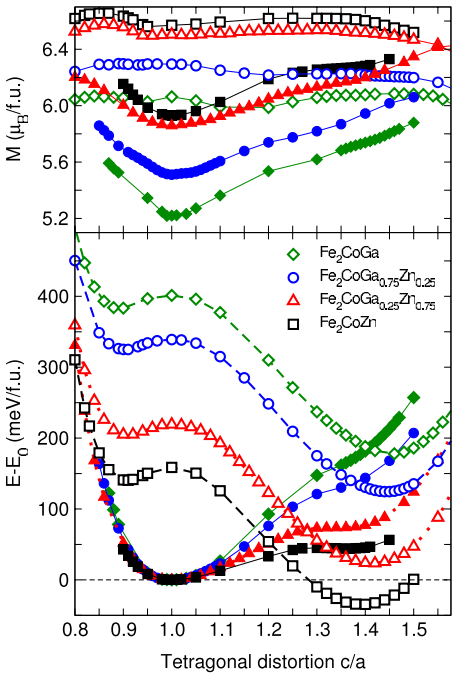

FIG. 2. (Color online) Total energy $E-E_0$ (lower panel) with respect to the energy of the cubic inverse structure for each alloy system and total magnetic moment M per f.u. (upper panel) of Fe_2CoGa (diamonds), $Fe_2CoGa_{0.75}Zn_{0.25}$ (circles), $Fe_2CoZn_{0.75}Ga_{0.25}$ (triangles), and Fe_2CoZn (squares) for both crystal structure types as a function of the tetragonal distortion, c/a. Open and filled symbols distinguish between the conventional and inverse Heusler structures, respectively. The conventional Heusler structures are characterized by two energy minima while the inverse structures show only one energy minimum in the cubic state ($c/a=1$). With increasing Zn concentration the energy of the conventional Heusler structure is considerably lowered approaching the energy curve of the corresponding inverse structure while the magnetic moments increase.

proved properties can be found in the literature. But little is known about Fe_2CoGa apart from the calculation of the total energy as a function of volume[36] and c/a ratio[37] and the hint of possible unstable $L2_1$ structure in Ref. 30. Material combinations including the element Zn have been investigated only very rarely so far. This work is a systematic first-principles study of this alloy series.

II. METHOD

Computational details

The self-consistent calculations of the structure, magnetism as well as the evaluation of force constants were carried out with the density-functional theory method as implemented in VASP using a plane-wave basis set and the projector augmented wave (PAW) method.[33,38] The exchange-correlation potential is used in the functional form of Perdew, Burke and Ernzerhof.[39,40] The PAW potentials include the following valence electrons: Fe: $3p^6 3d^7 4s^1$, Co: $3d^8 4s^1$, Ga: $3d^{10} 4s^2 4p^1$, and Zn: $3d^{10} 4s^2$. All plane waves with energies below the cut-off energy of 366.5 eV are included in the basis set. The integration over the Brillouin zone was carried out by means of the tetrahedron method with Blöchel corrections and a Γ-centered 13^3 grid. For the calculation of mixing energies we increased the number of k points to 19^3. The electronic self-consistency iteration cycle is aborted when the energy difference between two subsequent energies is less than 10^{-7} eV.

In a separate calculation, we have determined the magnetic-exchange interaction parameters, J_{ij}, by using the Munich spin-polarized relativistic KKR (SPR-KKR) package, version 3.6 with 250 k points and 30 energy points.[34,35] From these J_{ij} the Curie temperature is determined by means of Monte Carlo simulations of a classical Heisenberg model using the Metropolis algorithm. Periodic boundary conditions were used for system sizes up to 24^3 unit cells for a representative case. It turned out that a temperature step of 10 K, 100 Monte Carlo measurements per temperature step, and ten Monte Carlo sweeps in between two measurements were enough to obtain sufficiently smooth magnetization curves.

III. *AB INITIO* RESULTS

A. Structure optimization

From the results of total-energy calculations as a function of the lattice constant we determined for all systems the equilibrium lattice constants and magnetic moments which have been listed in Table I. For Fe_2CoGa experimental and theoretical data are available from literature[30,36,41] which is in good agreement with our calculations. A first check to assess the adequacy of the material for future FSMA applications is obtained from the variation in the energy landscape under a tetragonal distortion. During the continuous change in the c/a ratio along the Bain path,[42,43] the crystalline lattice transforms from the ideal $L2_1$ lattice ($c/a=1$) to the fcc-type closed-packed structure ($c/a=\sqrt{2}$). For the case that the material shows a tendency to undergo a martensitic transformation, usually two energy minima appear in the $E(c/a)$ curves, one near $c/a=1$ and a second one at $c/a>1$. Since the martensitic phase is the low-temperature phase, it may be associated with one of the energy minima observed in the *ab initio* calculations. The energy difference between the two local-energy minima is roughly proportional to the martensitic transformation temperature. In Fig. 2, the total energy with respect to the energy minimum of the cubic inverse phase for each system and the corresponding total magnetic moment, M, of all investigated $Fe_2CoGa_{1-x}Zn_x$ alloys are plotted as a function of the tetragonal distortion c/a.

We first discuss the ternary compounds Fe_2CoGa and Fe_2CoZn. It is obvious from Fig. 2 that for Fe-Co-Ga the inverse Heusler structure with only one energy minimum in the cubic state is the stable low-temperature phase. Thus, a martensitic transformation is not likely to occur for the inverse structure. This agrees well with the *ab initio* results of Gilleßen and Dronskowski[30] and the experimental findings of Jaggi *et al.*[32] In contrast to the inverse Heusler structure, the conventional Heusler structure, which lies higher in energy, shows the characteristic two energy minima of a structurally unstable system. The energy difference between the

TABLE II. Element-specific (in μ_B/atom) and total magnetic moment (in μ_B/f.u.) of the conventional and inverse Heusler structures for $c/a=1$. The magnetic moments do not change much when the cell is tetragonally distorted ($c/a \neq 1$). For comparison, the corresponding magnetic moments for the inverse cubic structures are added.

System	$M(Fe_A)$	$M(Fe_C)$	M(Co)	M(Ga)	M(Zn)	M
Conventional						
Fe_2CoGa	2.24	/	1.76	−0.08	/	6.15
$Fe_2CoGa_{0.75}Zn_{0.25}$	2.33	/	1.77	−0.08	−0.05	6.36
$Fe_2CoGa_{0.25}Zn_{0.75}$	2.45	/	1.76	−0.08	−0.05	6.60
Fe_2CoZn	2.50	/	1.74	/	−0.05	6.68
Inverse						
(FeCo)FeGa	1.79	2.59	1.08	−0.09	/	5.36
$(FeCo)FeGa_{0.75}Zn_{0.25}$	2.0	2.57	1.18	−0.10	−0.07	5.65
$(FeCo)FeGa_{0.75}Zn_{0.75}$	2.23	2.54	1.29	−0.11	−0.072	5.98
(FeCo)FeZn	2.30	2.52	1.32	/	−0.08	6.06

two minima is $\Delta E_{c/a}=55$ meV/atom (cf. Table I), which is almost four times larger than the energy difference of the prototypical compound Ni_2MnGa where $\Delta E_{c/a} \simeq 6$ meV/atom is found. Therefore, we may tentatively associate a higher martensitic transformation temperature with the ternary compounds Fe_2CoGa and Fe_2CoZn.

The compound Fe_2CoZn has one valence electron less than Fe_2CoGa. Interestingly, for Fe_2CoZn, the hierarchy of the two ordering types (conventional and inverse) has reversed (cf. Fig. 2). The conventional Heusler structure, which possesses two energy minima at $c/a<1$ and $c/a>1$, is now the lowest energy phase at $c/a=1.40$. But for the cubic phase ($c/a=1$) the inverse Heusler structure is still energetically preferred. Due to the competition of structures and due to the fact that during the experimental preparation procedure the specimens are cooled down from a disordered, cubic fcc structure (A1), it is not clear which of these two structures will evolve or whether eventually a completely disordered alloy may result. Also decomposition into a mixture of conventional and inverse structures is conceivable and the resulting energy landscape may still bear signatures of martensitic instabilities. This is especially interesting in the case of Fe_2CoZn, for which the absolute energy minimum at $c/a=1$ of the inverse Heusler structure lies only 9 meV/atom (36 meV/f.u.) higher in energy than the absolute energy minimum of the conventional Heusler structure at $c/a=1.40$. To remember, this energy is on the order of $\Delta E_{c/a}=6$ meV/atom of prototypical Ni_2MnGa. Therefore, any compositional changes including the influence of disorder may be important for the Fe-Co-Ga-Zn alloys and may drive the inverse alloys toward martensitically unstable systems, a prerequisite to observe the MSME. Experimental and theoretical work along these lines is in progress.

B. Magnetic moments and Curie temperatures

The upper panel in Fig. 2 shows that the conventional Fe_2CoGa and Fe_2CoZn compounds and corresponding substitutional alloys have larger or similar magnetic moments compared with the inverse systems, see Tables I and II. In conventional Fe_2CoGa each Fe has four Co nearest neighbors (nn) and four Ga nn while each Co has eight Fe nn. This yields 2.24 μ_B for Fe and 1.76 μ_B for Co. Zinc instead of Ga leads to a slightly enhanced Fe moment (2.50 μ_B) whereas Co remains unaffected (1.74 μ_B).

For the inverse structure we have two inequivalent Fe atoms. Fe_A has four Fe and four Ga nn whereas Fe_C has four Fe nn and four Co nn. This particular environment of Fe_C at the bcc-sublattice cube center and four Fe nn and four Co nn at the cube edges corresponds to the same environment as one of the Fe atoms in Fe_3Co (Ref. 18) and seems to favor the inverse over the conventional Heusler structure. For (FeCo)FeZn this leads to 2.30 μ_B for Fe_A and 2.52 μ_B for Fe_C and 1.32 μ_B for Co (Co has four Fe nn and four Zn nn which explains the rather low moment of Co in the inverse structure). The enhanced magnetic moments of Fe_A and Fe_C compared with the bulk value is similar to behavior of the spin moments of both Fe in Fe_3Co.[18] Since for the inverse structure the covalent interaction between Fe nn and Co nn is strong in each spin channel, it bears features of covalent magnetism as in FeCo,[18] which finally lowers the total energy of the inverse structure compared with the conventional one. This is detailed below in the discussion of the electronic structure.

Figure 2 also shows that in the inverse $(XY)XZ$ structure the total moments follow the overall trend found in the energy profile and show a well-defined minimum for the cubic state. Comparing conventional Fe_2CoGa and Fe_2CoZn we may tentatively conclude that the reduced occupation of the minority-spin channel of Fe_2CoZn (Zn has one valence electron less than Ga) gives rise to the enhanced total moment of the Zn-based compounds. It is clear from the present investigation that Fe favors a bcc-like environment in Fe_2CoGa and Fe_2CoZn as it is the case for other magnetic Heusler alloys with two inequivalent Fe as in Fe_3Co (Ref. 18) and Fe_3Si.[44] However, only in the inverse structures the strong ferromagnetic nearest-neighbor Fe_C-Fe_A and Fe_C-Co interactions can evolve (cf. Fig. 3).

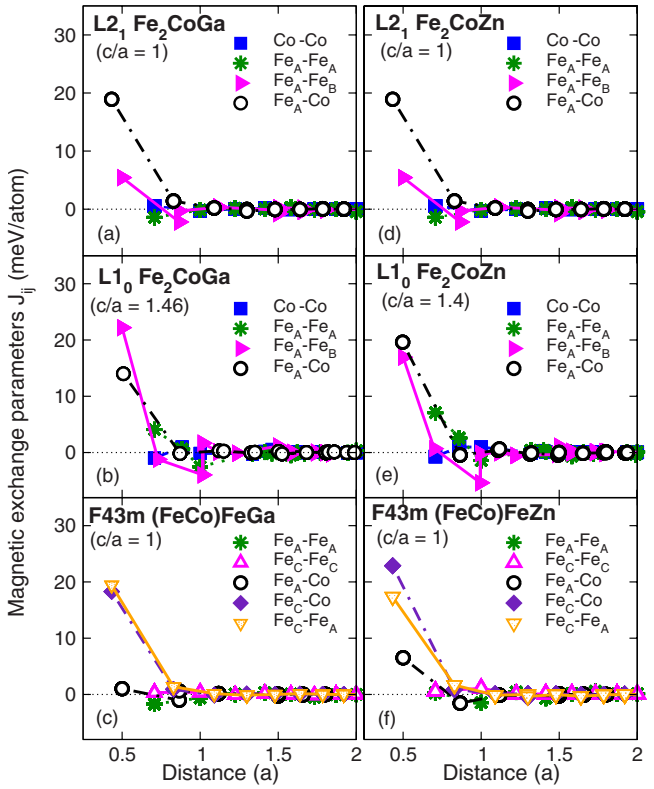

FIG. 3. (Color online) Magnetic-exchange parameters J_{ij} as a function of the distance d between the atoms in units of the equilibrium lattice constant a_0 for the cubic cases ($c/a=1$) and in units of a for the tetragonal structures for (a) $L2_1$ Fe_2CoGa ($c/a=1$), (b) $L1_0$ Fe_2CoGa ($c/a=1.46$), (c) inverse $F\bar{4}3m$ (FeCo)FeGa ($c/a=1$), (d) $L2_1$ Fe_2CoZn ($c/a=1$), (e) $L1_0$ Fe_2CoZn ($c/a=1.40$), and (f) inverse $F\bar{4}3m$ (FeCo)FeZn ($c/a=1$). The distance is given with respect to the first atom in the figure legend. For the Fe_x-Fe_y interaction ($x,y=$A,B,C) there is always an Fe_x atom at the origin, for the Co-Co interactions a Co-atom occupies the origin. Squares (blue) mark the interaction between two Co atoms, stars (green) define the Fe_A-Fe_A interactions, filled rightward triangles (magenta) belong to the Fe_A-Fe_B interactions, and open circles (black) mark the interactions between Fe_A and Co. Open upward triangles (magenta) indicate the Fe_C-Fe_C interaction, filled diamonds (indigo) show the Fe_C-Co interactions, and downward triangles (orange) the Fe_C-Fe_A interactions. The strongest interactions are ferromagnetic and appear between Fe atoms and Fe and Co atoms.

As mentioned before, for future exploitation of the MSME the materials should possess Curie temperatures which are considerably higher than room temperature in order to guarantee operation of devices and actuators at elevated temperatures. In order to check this requirement for the materials discussed in this paper, we have calculated the magnetic-exchange parameters and the resulting Curie temperatures which are shown in Fig. 3 and Table I for the respective cases of Fe_2CoGa and Fe_2CoZn. In the upper panels the magnetic coupling constants are given for the conventional and in the lower panel for the inverse structures. The magnetic-exchange coupling constants show strong ferromagnetic coupling of Fe_A-Co and Fe_A-Fe_B pairs of atoms in the conventional and between Fe_C and Co atoms and Fe_C and Fe_A atoms in the inverse structure. This results in rather high Curie temperatures between 770 and 925 K (cf. Table I). In the tetragonally distorted conventional Heusler structure also slight antiferromagnetic tendencies appear regarding the Fe_A-Fe_B interactions, which show up at distances of one lattice constant. The highest Curie temperature of 925 K is found for the conventional Fe_2CoZn compound. This enhancement of about 150 K compared to $T_C=770$ K of the conventional Fe_2CoGa compound is caused by the increased Fe_A-Fe_A coupling and goes hand in hand with the enhancement of the total magnetic moment of Fe_2CoZn.

The foregoing discussion shows that, when replacing Ga by Zn, the Curie temperature can be increased. Therefore, coalloying of Zn may be beneficial for future FSMA in order to achieve higher operation temperatures. The origin of the enhanced magnetic moment in the Zn-based compounds will be discussed in Sec. III F.

C. Mixing energies

In order to gain information about the structural stability and decomposition tendencies of the compounds, we have determined the mixing energies. The mixing energy can be easily obtained by subtracting from the ground-state energy of the alloy system the total sum of the bulk energy of material component i weighted by its concentration c_i

$$E_{\mathrm{mix}} = E_{alloy} - \sum_i c_i E_i. \tag{1}$$

Negative mixing energies indicate that the alloys are stable against spinodal decomposition into their elemental constituents. This does not imply stability against compounds arising from various combinations of the constituents (which are too numerous to consider systematically) but provides meaningful trends with respect to changes in composition. For all investigated alloys, except for stoichiometric Fe_2CoZn, the mixing energies are negative (cf. Table I). With increasing Zn concentration in quaternary $Fe_2CoGa_{1-x}Zn_x$ systems the mixing energy increases. The positive mixing energy of stoichiometric Fe_2CoZn and simultaneous presence of a martensitic instability is essentially caused by zinc and bears resemblances to the spinodal and martensitic regions in the ternary phase diagram of the nonferrous Cu-Zn-Al Heusler alloy system.[45]

D. Quaternary alloy systems $Fe_2CoGa_{0.75}Zn_{0.25}$ and $Fe_2CoGa_{0.25}Zn_{0.75}$

We have shown that the ternary compound Fe_2CoGa provides high Curie temperatures but the low-temperature phase is the inverse structure which is not martensitic. In the related alloy series the replacement of Ga by Zn has led to enhanced Curie temperatures, reduced the energetic preference of the inverse Heusler structure and the miscibility. In order to find an alloy with optimized material properties and to clarify the effect of Zn on the structural stability, we present the systematic investigation of trends associated with successive addition of Zn in the quaternary system $Fe_2CoGa_{1-x}Zn_x$.

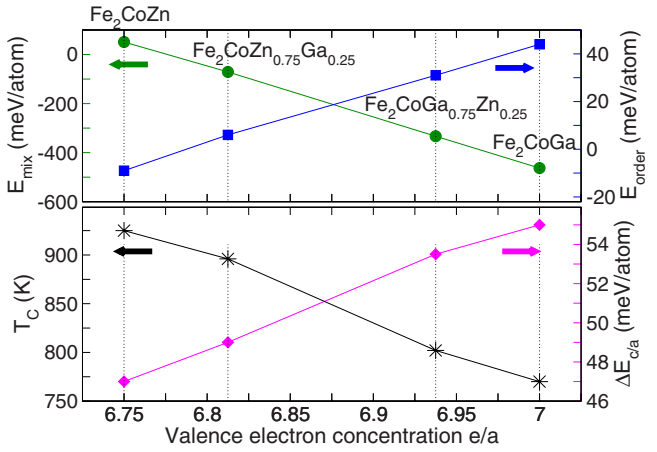

FIG. 4. (Color online) The influence of addition of Zn to Fe_2CoGa in the conventional tetragonally distorted Heusler structure ($L1_0$) on the Curie temperature T_C (left axis, lower panel), the energy difference between the cubic phase at $c/a=1$ and the absolute energy minimum at $c/a>1$, $\Delta E_{c/a}$ (right axis, lower panel), the mixing energy, E_{mix} (left axis, upper panel), and the energy difference between the absolute energy minima of the conventional and the inverse phases, E_{order} (right axis, upper panel), as a function of the valence-electron concentration e/a. All functional behavior depends linearly on e/a.

The effect of addition of zinc on the energy landscape and on the total magnetic moment when passing from Fe_2CoGa and $Fe_2CoGa_{1-x}Zn_x$ to Fe_2CoZn can be discussed on the basis of Fig. 2. Two remarkable modifications are observed. First, Zn reduces considerably the energetic preference of the inverse cubic structure in favor of the tetragonally distorted conventional structure. In the ternary compound Fe_2CoGa the energy difference between the absolute energy minima of inverse structure and conventional structures, ΔE_{order}, amounts to 44 meV/atom. This difference reduces to 31 meV/atom for $Fe_2CoGa_{0.75}Zn_{0.25}$ and to 6 meV/atom in $Fe_2CoZn_{0.75}Ga_{0.25}$. Finally, for Fe_2CoZn this energy difference reverses its sign yielding −9 meV/atom. This trend emphasizes that now the tetragonal conventional Heusler structure is the energetically preferred phase (cf. Table I and Fig. 4). Nonetheless, considering the cubic case ($c/a=1$) we find that the inverse structure is still favored for all compositions. Another observation is important. The substitution of Zn for Ga does not significantly modify the energy profile of $E(c/a)$ of the conventional Heusler systems, contrary to the inverse structures for which the tendency of a second-energy minimum at $c/a>1$ becomes significantly more pronounced as more Zn is added. This implies that the inverse structures become elastically softer, which influences the magnetostrictive coefficient $\lambda_{[001]}$ of the cubic phase of the Heusler alloys. Regarding the effect of softer elastic behavior when substituting Zn for Ga in Fe_2CoGa we note that this is in good agreement with results obtained by Wu and co-workers[15] who found that the magnetostrictive coefficient $\lambda_{[001]}$ of $Fe_{87.5}Ga_{12.5}$ can be further enhanced by the substitution of Zn for Ga. The softening of the inverse structure with increasing amount of zinc is also reflected in the phonon dispersions, see Fig. 5. The frequencies of the lowest acoustical branch of (FeCo)FeZn are significantly lower compared with (FeCo)FeGa along the [110] direction. As for the ternary compounds Fe_2CoGa and Fe_2CoZn, we find strong ferromagnetic coupling in the $Fe_2CoGa_{1-x}Zn_x$ alloys and the Curie temperatures are high, $T_C=768$ K for $Fe_2CoGa_{0.75}Zn_{0.25}$ and $T_C=830$ K for $Fe_2CoGa_{0.25}Ga_{0.75}$ (cf. Table I). The mixing energies remain, despite the addition of Zn, negative for both ordering types (conventional and inverse).

In Fig. 4 we summarize the influence of the stepwise addition of Zn to $L1_0$ Fe_2CoGa on the Curie temperature, the energy difference between the cubic phase at $c/a=1$ and the energy minimum at $c/a>1$, $\Delta E_{c/a}$, the mixing energy, E_{mix}, and on the energy difference between favorable structures of conventional and inverse phases, ΔE_{order}. The Curie temperature increases almost linearly with increasing Zn content (decreasing e/a ratio), simultaneously, $\Delta E_{c/a}$ decreases only slightly. These are desirable results in order to enhance the operation temperatures of future FSMA. The mixing energy

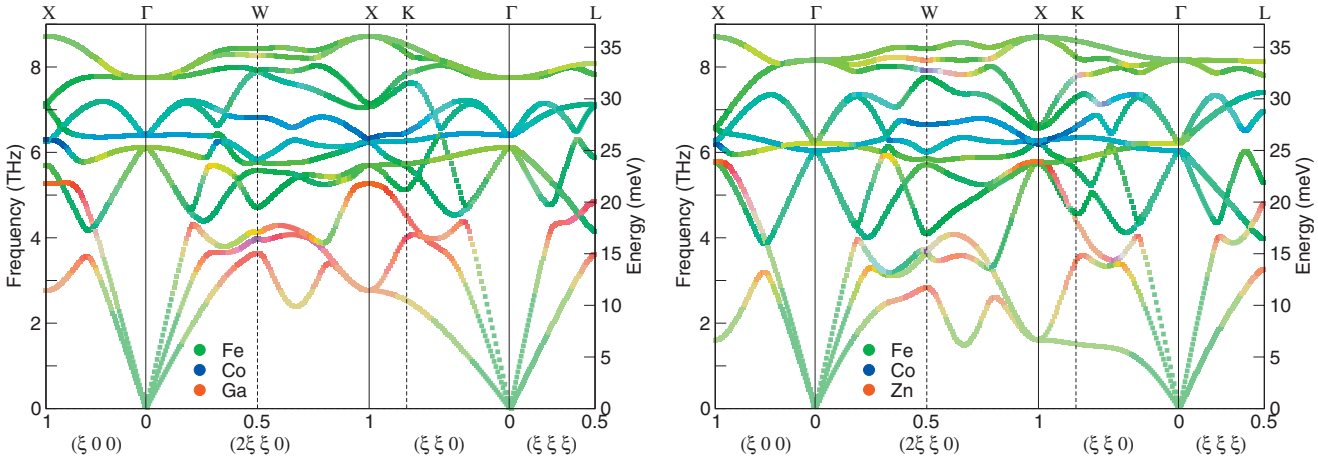

FIG. 5. (Color) Phonon-dispersion relations of the inverse cubic Heusler compounds (FeCo)FeGa (left) and (FeCo)FeZn (right). For the inverse structure involving zinc, a tendency for phonon softening is observed regarding the TA_2 mode in [110] direction but no imaginary phonons are apparent, contrary to the conventional cubic systems $Fe_2Co(Ga,Zn)$ (not shown). For the latter compounds the negative curvature of $E(c/a)$ at $c/a=1$ causes instabilities in the [110]-TA_2 phonon branch.

shows a perfect linear increase with decreasing e/a ratio while ΔE_{order} decreases steadily which establishes the stabilization of the conventional Heusler structure with increasing amount of Zn. The remarkably linear dependence of all functional properties on the valence-electron concentration e/a hints toward the possibility of discussing the results in a rigid bandlike picture. This will be used in Sec. III F to obtain further qualitative understanding, in particular, of the role of covalent magnetism in favor of the inverse structures. To summarize, successive substitution of Zn for Ga in Fe_2CoGa is beneficial for enhancing the Curie temperature and for the stabilization of the conventional Heusler structure while simultaneously the martensite transformation temperature, which is proportional to $\Delta E_{c/a}$, can be kept high. Although the fabrication of Zn-rich $Fe_2CoGa_{1-x}Zn_x$ samples with slightly negative mixing energies will be demanding, we think that the system has promising properties which make it worthwhile for systematic experimental investigation. From the theoretical point of view, further investigation of the role of disorder in $Fe_2CoZn_{0.75}Ga_{0.25}$ is necessary to establish the relation between flat energy profiles and high Curie and martensite transformation temperatures.

E. Lattice dynamics

In the prototype FSMA Ni_2MnGa a softening of the [110]-TA_2 phonon branch can be observed experimentally as well as theoretically and is often considered as a precursor phenomenon of the premartensitic or martensitic transformation, although, in general, it is not a mandatory precondition for the occurrence of a martensitic transformation. In order to clarify whether phonon softening also appears in $Fe_2Co(Ga,Zn,Cu)$, the full phonon spectra of Fe_2CoGa, Fe_2CoZn, and, in addition, Fe_2CoCu (discussed in Sec. III H) have been calculated for the conventional as well as for the inverse Heusler structures. The phonon dispersion curves were calculated using the PHON code of Dario Alfè which makes use of the so-called direct approach,[46] where the force constants needed to achieve the dynamical matrix were obtained from supercell calculations using 108 atoms (3^3 primitive cells). According to the symmetry of the primitive cell, atoms were individually displaced from their ideal positions by 0.02 Å and the resulting forces were calculated using a 2^3 Monkhorst grid as a k mesh. The dispersions were calculated for the conventional and the inverse structures. Because of negative curvatures of the total energies upon tetragonal distortions in the vicinity of $c/a=1$ in case of conventional structures, imaginary dispersions are obtained for the lattice vibrations in [110] direction. These dispersions are not shown here. Instead, we show in Fig. 5 the computed phonon-dispersion relations of the inverse cubic structures for the ternary systems (FeCo)FeGa and (FeCo)FeZn along the [110] direction. The most remarkable difference between (FeCo)FeGa and (FeCo)FeZn is the frequency of the lowest acoustic branch that can be found at the X point. While the position of the other branches does not differ much between the two materials, a significant decrease of the frequency at the zone boundary can be observed for (FeCo)FeZn. For (FeCo)FeCu (not shown here) imaginary frequencies can be observed along the [110] direction at a wave vector rather similar to the vector where the phonon softening in Ni_2MnGa appears. As imaginary frequencies do not appear in other regions of the Brillouin zone and since the position of the involved branch near the zone boundary and also the frequencies of the other branches do not change significantly, the imaginary frequencies along the [110] direction could indeed be an indication of an anomalous temperature dependence of phonon softening in (FeCo)FeCu in the vicinity of a martensitic instability.

The fact that the frequencies of the acoustic branches decrease with decreasing valence-electron concentration e/a is in contrast to findings for other material classes such as Ni_2MnZ, Ni_2CoZ, or Co_2MnZ as it has been shown that the nearest-neighbor force constants decrease linearly with increasing e/a ratio for these Heusler compounds.[47]

F. Electronic structure

We have shown in Sec. III D that in all investigated compounds Fe_2CoGa, Fe_2CoZn and structures with mixture of Ga and Zn, the inverse structure is always more stable than the conventional Heusler phase at $c/a=1$. For the Fe_2CoGa and the $Fe_2CoGa_{1-x}Zn_x$ systems, the inverse structure is even more favorable than the tetragonally distorted conventional Heusler phase. Remarkable is the linear reduction in the energy difference between the conventional and the inverse Heusler structure, ΔE_{order}, with increasing Zn content in $Fe_2CoGa_{1-x}Zn_x$. Hence, addition of zinc stabilizes the tetragonal conventional phases. This raises several questions: (i) what causes the instability of the cubic conventional $L2_1$ structure and what is the origin of the tetragonal distortion? (ii) When Zn is substitutionally replacing Ga, what causes the reduction in the energetic preference of the cubic inverse structure in favor of the tetragonally distorted conventional one? (iii) What is the reason for the high stability of cubic inverse structure and why are all conventional $Fe_2CoGa_{1-x}Zn_x$ structures martensitic and the inverse ones not? (iv) When increasing the Zn content in inverse (FeCo)$FeGa_{1-x}Zn_x$ alloys, what causes the trend for a second minimum in the $E(c/a)$ curves [filled triangles and squares in Fig. 2]? (v) Also the enhanced magnetic moments with increasing zinc content need to be understood.

In order to clarify these issues, we have calculated band structures and the electronic density of states of conventional and inverse structures. (i) Some explanations can be obtained from the literature, the combinatorial study of inverse and conventional Heusler alloys by Gilleßen and Dronskowski[30] shows that the transformation from the conventional to the inverse structure occurs most easily whenever the atoms have similar (or identical) sizes (this holds for Fe and Co in the present study). In their analysis of chemical bonding in Fe_2CuGa, using the crystal-orbital Hamilton population concept[48] in the framework of the all-electron scalar-relativistic linear muffin-tin orbital method, they could show that the driving force for adopting the inverse Heusler phase, for example, in Fe_2CuGa results from strengthening of nn Fe-Fe and Cu-Ga bonds. This happens because the nn distance of Fe-Fe and Cu-Ga is drastically reduced compared

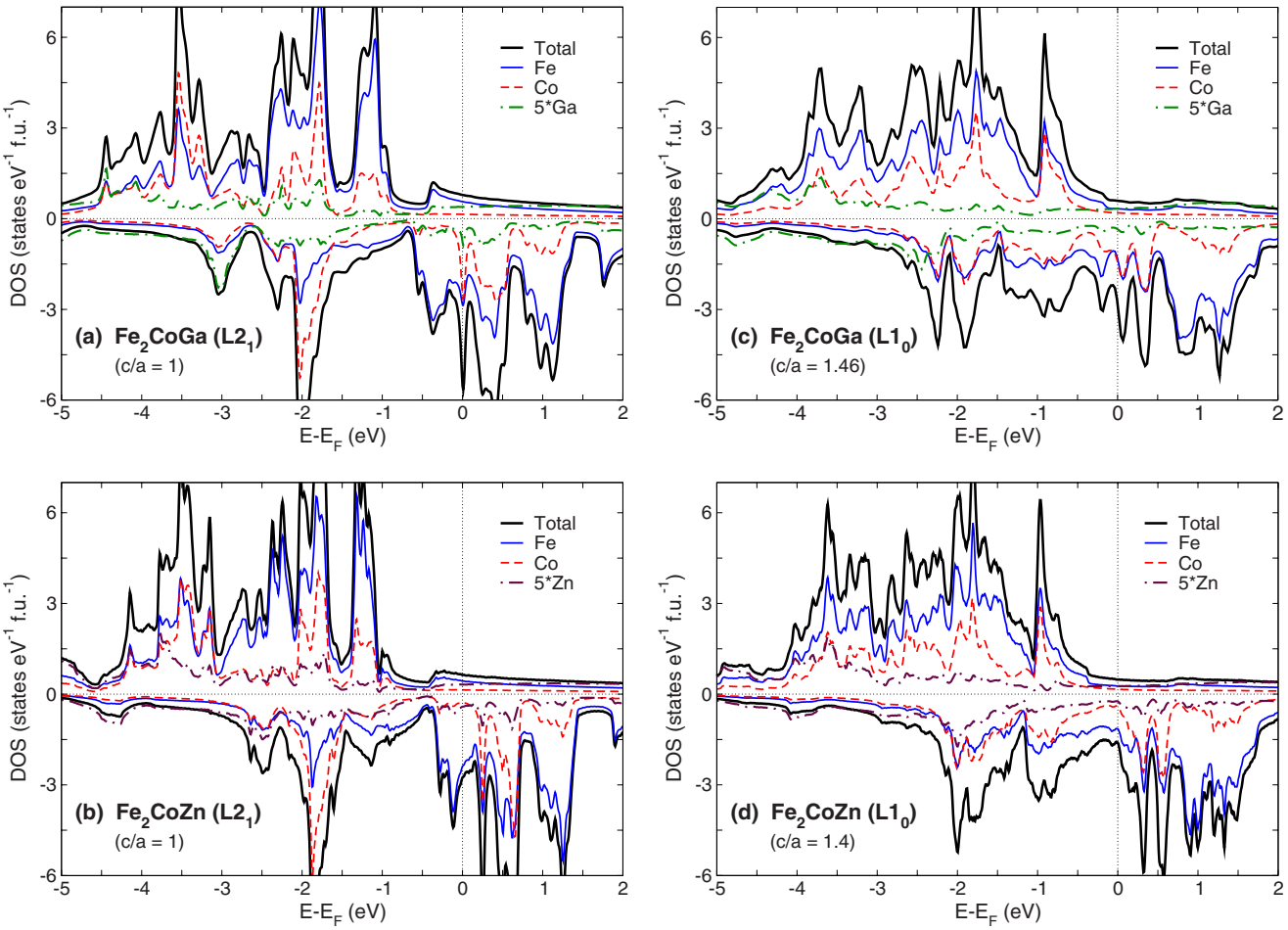

FIG. 6. (Color online) The two figures on the left show the total and element-specific DOS of the cubic $L2_1$ phases of (a) Fe_2CoGa and (b) Fe_2CoZn while the two figures on the right show the corresponding total and element-specific DOS of the tetragonal $L1_0$ phases of (c) Fe_2CoGa and (d) Fe_2CoZn. The high peak at the Fermi level in the spin-down channel in case of Fe_2CoGa is of Co e_g origin and mainly responsible for the instability of the ordered conventional phase and may also favor the tetragonal distortion (band-Jahn-Teller effect) thereby lowering the energy of the $L1_0$ phase with respect to the $L2_1$ phase. For Fe_2CoZn a peak of mainly Fe e_g and Fe t_{2g} lies right below E_F (as in case of $L2_1$ Ni_2MnGa) which in this case is responsible for the instability. Note that for the $L1_0$ phase of both compounds the gaplike region of the cubic phase below E_F is now filled with states of Co and Fe. The thicker solid (black) lines show the total DOS, thinner (blue) lines belong to Fe (for $L1_0$ this is the sum of contributions from the two inequivalent atoms Fe_A and Fe_C), dashed (red) lines mark the Co states, dashed-dotted (green) lines represent Ga and Zn (maroon), respectively. For better visibility the DOS of Ga and Zn is enhanced by a factor of 5.

with their corresponding distances in the conventional structure, where they are only next-nearest neighbors. However, regarding tetragonal distortions, the conventional structure of Fe_2CuGa, when distorted, is even lower in energy than the inverse cubic structure. This has been explained by the observation that Fe-Ga and Fe-Cu bonds which became weaker in the inverse cubic structure due to the loss of nearest-neighbor coordination, regain strength while the short Fe-Fe and Cu-Ga bonds of the inverse structure are preserved. Gilleßen and Dronskowski found that, in general, Heusler compounds with a valence-electron concentration $e/a < 7.25$ prefer the inverse cubic atomic arrangement while for those with an e/a ratio larger than 7.25 the tetragonal (inverse or conventional) arrangement of atoms is most favorable. Their results confirm the general trend of our findings since for all $Fe_2CoGa_{1-x}Zn_x$ alloys $e/a < 7.25$ holds for which the inverse structure is most favorable at $c/a = 1$ while for the $Fe_2Co(Cu,Ag,Au)$ compounds discussed in Sec. III H $e/a > 7.25$ holds and the energetically favorable structure is tetragonal. The only exception is Fe_2CoZn with $e/a = 6.75$. But note that Fe_2CoZn has a positive mixing energy and is unstable with respect to spinodal decomposition.

Information about the electronic structure can be gained from the electronic density of states shown in Figs. 6–8. In Fig. 6 we present the total and element specific DOS for the cubic and the tetragonal phases of conventional and in Fig. 7 of inverse cubic structures, respectively. In addition, we show the e_g and t_{2g} contributions of Fe and Co in Fig. 8. A similar analysis has been done for the Ga-Zn-mixed phases where the DOS interpolates smoothly between the pure cases, Fe_2CoGa ($e/a = 7.0$) and Fe_2CoZn ($e/a = 6.75$). These figures are not shown here. Figures 6(a) and 6(b) shows the energetically unfavorable $L2_1$ structures and the corresponding energetically preferred $L1_0$ structures in Figs. 6(c) and

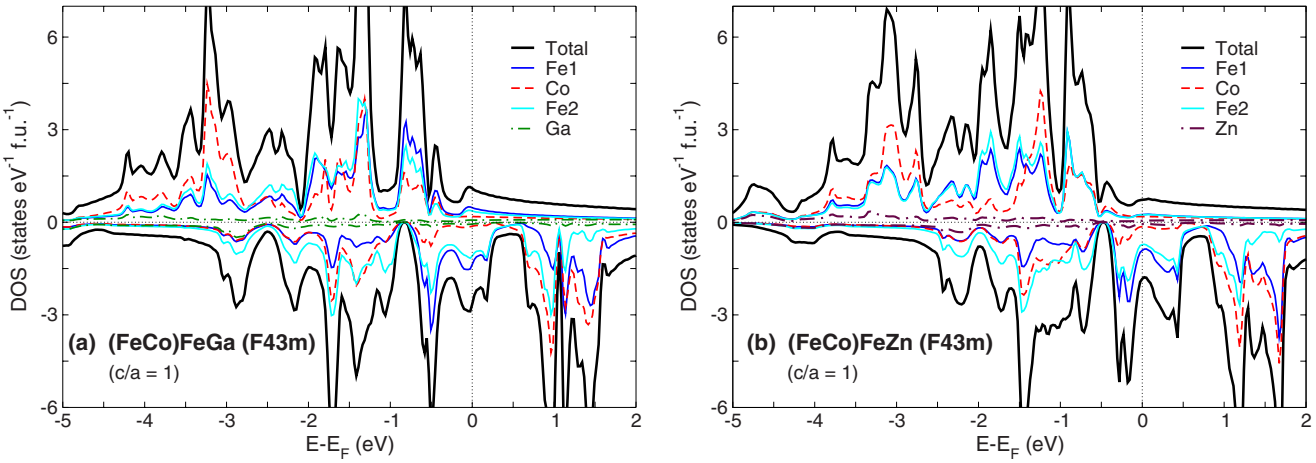

FIG. 7. (Color online) The DOS of the inverse structures for the cubic case for (a) (FeCo)FeGa and (b) (FeCo)FeZn. The individual contributions of both inequivalent Fe are shown in blue and violet. There are two pseudogap structures below (−0.8 eV) and above (0.5 eV) the Fermi level. The DOS of the minority-spin appears rather compressed and the peak structure at E_F has disappeared compared with the conventional case.

6(d). In this context one has to note that zinc has no p electron and thus one valence electron less than gallium.

For all $L2_1$ phases the DOS of the minority spins at the Fermi level is quite high, especially for Fe_2CoGa [cf. Fig. 6(a)], where a sharp peak consisting of mainly Co and Fe states appears right at E_F similar to the case of the prototypical compound Ni_2MnGa. This is a hint that the system may undergo a structural transformation which leads to a region of small width of reduced DOS around E_F. The redistribution of spin-up and spin-down electrons may then lower the energy of the tetragonal structure with respect to the cubic structure which was discussed previously in terms of the band-Jahn-Teller effect for Ni_2MnGa.[49] In case of Fe_2CoGa, this redistribution is most clearly visible, the peak structure at E_F and further states below and above E_F develop a multivalley structure of reduced Fe and Co DOS in the tetragonal phases. As for the prototypical compound Ni_2MnGa, the peak of high DOS at E_F in the cubic phase is then shifted above E_F with much lower spectral weight in the tetragonal phase. Thus, the martensitic transformation in Fe_2CoGa and Ni_2MnGa has the same origin.

The e_g and t_{2g} decomposed states in Fig. 8 show more clearly the states which are responsible for the instability of the conventional cubic phase. Figure 8(a) shows that Co e_g states contribute most of the spectral weight to the sharp peak at E_F in Fe_2CoGa which therefore is responsible for energy lowering by the band-Jahn-Teller effect upon a small tetragonal distortion. This explains the stability of the $L1_0$ phase relative to the cubic phase of Fe_2CoGa. Regarding the $Fe_2CoGa_{1-x}Zn_x$ systems the stability of the $L1_0$ phase has the same physical origin.

Another aspect concerns the occurrence of a pronounced pseudogap, for Ni_2MnGa we find this gaplike structure below E_F (just below the high DOS peak with Ni e_g spectral weight) whereas for the cubic phases of Fe_2CoGa and Fe_2CoZn we observe two pseudogaps, one at 0.7 eV below E_F and another one at 1.5 eV above E_F. In Ni_2MnGa this near-semiconducting gap or pseudogap is caused by the missing hybridization of t_{1u} and e_u states of Ni with t_{2g} and e_g states of Mn due to the different symmetries of the crystal fields of octahedrally coordinated Ni (in our case Fe) and tetrahedrally coordinated Mn (in our case Co). See also the discussion in Ref. 50 regarding the origin of the half metallicity of the full-Heusler alloys. This kind of gap structure is filled up with Co and Fe states in the tetragonal $L1_0$ phases of Fe_2CoGa and also Fe_2CoZn.

(ii) Another interesting effect is observed in the $L1_0$ structure when substituting Zn for Ga. With increasing Zn concentration the Co minority-spin DOS at E_F of predominantely antibonding e_g and t_{2g} states is gradually reduced until finally E_F is pinned in a valley for $L1_0Fe_2CoZn$. This is responsible for the approximately linear decrease in ΔE_{order} with decreasing e/a (increasing Zn concentration) (cf. Figs. 2 and 4). The hybridization of the Fe d and Co d states with sp states of Ga and Zn also leads to peak structures which are here only mentioned (the Zn d band lies 7.5 eV below E_F and does not effect the Fe-Co hybridization too much). Part of the conduction-electron s states of zinc strongly hybridize with Co d and Fe d states giving rise to the peak structures at about −4.1, −3.8, and −1.8 eV in the majority-spin DOS and at 0.3 eV in the minority-spin DOS.

Thus, we can conclude that the enhanced stability of the tetragonally distorted $L1_0$ phase compared to the cubic inverse phase for the Zn-rich alloys can be explained by stronger Co-Zn and Fe-Zn interactions due to stronger hybridization with zinc s. This is in good agreement with the results of Gilleßen and Dronskowski who found that in the tetragonal $L1_0$ phase of the conventional structure the Fe-Z bonds regain strength.

(iii) We still need to understand the preference of the cubic phase of the inverse structure ($c/a=1$) over the conventional structure and the absence of any sign of structural instability. In this context it is helpful again to compare the DOS of conventional and inverse structures at $c/a=1$ in Figs. 6(a), 6(b), and 7. Interestingly, for the inverse cubic structures the pseudogap structure in the minority-spin channel (at about −0.8 eV for Fe_2CoGa) is much more pronounced and a second pseudogap at energies above E_F

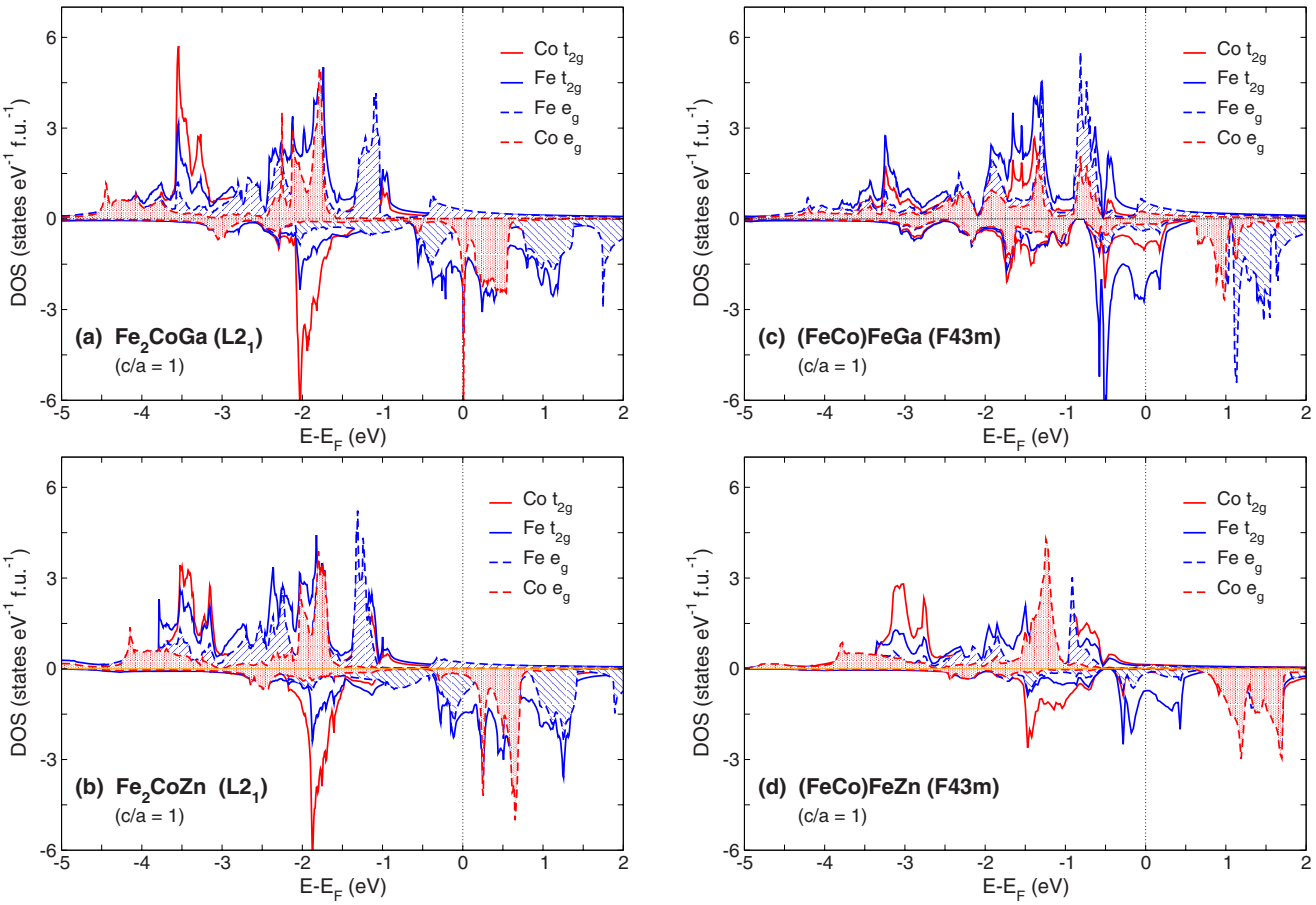

FIG. 8. (Color online) The e_g and t_{2g} decomposed DOS of conventional (a) Fe_2CoGa and (b) Fe_2CoZn showing the peak structure near the Fermi level which is responsible for the martensitic instability in both systems. The peak structure is less pronounced in case of Fe_2CoZn. Note also the extra spectral weight of Fe at energies above E_F and the extra spectral weight of Co at 2 eV below E_F in the minority-spin states which bears features of covalent magnetism as in CoFe, see Ref. 18. Figs. 8(c) and 8(d) show the e_g and t_{2g} decomposed DOS of the corresponding inverse Heusler compounds. The peak structure at E_F has vanished and the DOS is rather different compared with the conventional structures.

evolves [at about 0.5 eV for (FeCo)FeGa]. A pseudogap in the minority-spin channel appears also for other inverse structures such as (FeCo)FeSi and (CoFe)CoSi.[51] The inverse structures show stronger hybridization of Co and Fe states due to the fact that in the inverse phase one Fe is interchanged with Co, see Fig. 1 so that now both, Fe and Co atoms, are subject to the same crystal field of tetrahedral symmetry which splits their d orbitals only into t_{2g} and e_g symmetries and no longer into t_{2g} and t_{1u} and e_g and e_u symmetries as in the case of the crystal field of octahedral symmetry which acts on the Fe atom in the conventional structure. Due to symmetry reasons the hybridization is forbidden between antibonding states with u symmetry and bonding states with g symmetry.[50] Note, however, that this complex hybridization scenario does not lead to specifically low DOS at E_F for the inverse structures compared with the conventional ones. Furthermore, the DOS of the tetragonal inverse structures (not shown here) reveals that (as for the tetragonal conventional phases), the bump in the majority-spin-channel above E_F which causes a bit of Fermi-surface nesting for the spin-up electrons (not shown here) is dissolved and pseudogaps are filled with states although the inverse structures do not show a second-energy minimum at $c/a>1$. This implies that the inspection of the DOS alone is insufficient to explain the stability of the inverse structures at $c/a=1$.

Therefore, we have checked the coordination and nearest-neighbor relations in conventional and inverse atomic arrangements. In the inverse phase two different types of Fe exist, Fe_A and Fe_C (cf. Fig. 1). Fe_C is tetrahedrally coordinated by four nn Fe_A and four nn Co while Fe_A possesses Ga instead of Co as nearest neighbors. However, in the conventional cubic phase Fe atoms are only next-nearest neighbors with octahedral coordination and build an unfavorable simple cubic Fe sublattice if one neglects for a moment Y and Z atoms in the unit cell. In the conventional cubic $L2_1$ structure, the nn of Fe are four Ga and four Co atoms. Thus, only in the cubic inverse structure Fe_C can adopt a bcc-like environment of transition-metal atom neighborhood. This is the reason for the remarkable energetic preference of the inverse cubic structure in case of Fe-Co-Ga alloys. This tendency of Fe to prefer a bcc-like environment is also found in the studies of Co-Fe-Si alloys by Herper.[51] The authors observed that (FeCo)FeSi prefers an inverse atomic arrangement while Co_2FeSi is stable in the conventional $L2_1$ phase. This originates from the fact that Co atoms, in contrast to Fe

atoms, prefer a more close-packed, fcc (or hcp) neighborhood and agrees well with the experimental study of Fe-Co-Ga alloys by Jaggi *et al.*,[32] and the *ab initio* investigation of Fe-Cu-Ga alloys by Gilleßen and Dronskowski.[30] One is tempted to consider other transition-metal-rich Heusler alloys (with transition metals right to Fe in the periodic table) and check whether similar trends can be observed. For example, the stability of inverse and conventional structures of Ni_2MnGa (Ref. 52) and Co_2NiGa.[53] For Ni_2MnGa the situation is opposite compared with Fe_2CoGa, i.e., the conventional structure is energetically clearly preferred at $T=0$ K which confirms our assumption. Furthermore, in off-stoichiometric Ni-Mn-Ga alloys, nn Ni-Mn pairs are energetically preferred, although, the situation is more complex because of the change from ferromagnetic to antiferromagnetic order. Regarding Co_2NiGa, we encounter a competition of different ordering mechanisms because both, Ni and Co atoms, prefer a fcc-like crystal structure in their elemental phase. And indeed, this is reflected in the calculations. Inverse and conventional cubic phase are almost degenerate and may thus lead to an inherent preference for disordered arrangements.

This favorable atomic arrangement found for Fe and Co atoms in the cubic inverse structure implies that there is no need for the material to undergo a structural transition to a tetragonal distorted phase.

(iv) When Zn is replacing Ga the strong Fe-Co hybridization in the inverse structure is weakened and the stability of the cubic inverse structure is reduced enhancing the tendency for a second-energy minimum at $c/a>1$. The origin is the competing hybridization of Zn s electrons with Co d and Fe d electrons as already discussed above in the framework of the increasing stability of the $L1_0$ phase for the Zn-rich alloys. Thus, the almost linear reduction in ΔE_{order} when Zn is substitutionally replacing Ga has the same origin as the enhanced tendency for a martensitic instability in the Zn-based inverse systems.

(v) Again, one has to bear in mind that Zn has one valence electron less than Ga. Because of the strong hybridization of Fe d and Co d with Zn s states, the effect of lower e/a when replacing Ga by Zn, leads to a shift of the whole minority-spin DOS upward in energy while significant features as, e.g., the peak at −2 eV and the peak at E_F remain almost unchanged for Fe_2CoZn. As a consequence the total magnetic moment increases.

G. Covalent magnetism

Figure 9(a) shows the actual DOS of $L2_1$ Fe_2CoGa obtained by self-consistent *ab initio* calculation of the majority-spin DOS and in Fig. 9(c) of the minority-spin DOS in comparison with the Stoner-type minority-spin DOS in Fig. 9(b) obtained by a rigid-band shift of the inverted spin-up states under maintenance of the total magnetic moment. It is clearly visible in Fig. 9(a) that in the majority-spin DOS Fe and Co have more or less the same spectral weight per atom and do not differ too drastically from each other (note that the DOS of Fe in Fig. 9 is twice of that of Co because there are two Fe per formula unit). The majority-spin DOS also

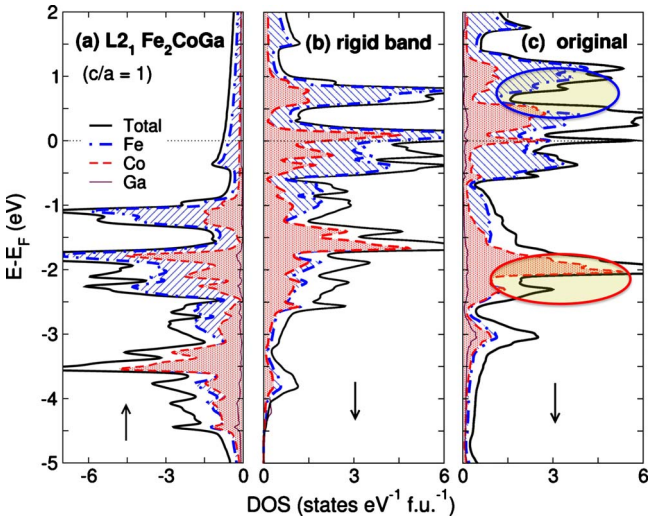

FIG. 9. (Color online) (a) Majority-spin density of states of $L2_1$ Fe_2CoGa as obtained by self-consistent *ab initio* calculations showing that the DOS per atom of Fe and Co are very similar. (b) Minority-spin DOS of the rigid band picture of the Stoner model in case of $L2_1$ Fe_2CoGa compared with (c) the actual minority-spin DOS of $L2_1$ Fe_2CoGa. The influence of covalent interaction (hybridization) in the minority-spin channel in case of (c) is clearly different from the rigid-bandlike picture in (b) and is the cause of covalent magnetism similar to the case of FeCo discussed in Ref. 18. We have, however, to keep in mind that the different crystal fields acting on Fe (octahedral) and on Co (tetrahedral) have also influence on the detailed shape of the minority-spin DOS of $L2_1$ Fe_2CoGa.

bears resemblance to the majority-spin DOS of bcc Fe and bcc FeCo by showing a clear subdivision of the DOS in the majority-spin channel into bonding, nonbonding, and antiboding regions, which has been discussed in detail by Schwarz *et al.*[18] Also shown is the different minority-spin DOS of Fe_2CoGa. The strong covalent interaction in both spin channels just as in case of FeCo (Ref. 18) is clearly visible. As in FeCo, this leads to large additional DOS of Fe at $E>E_F$ and large additional spectral weight of Co at −2 eV in the minority-spin DOS of Fe_2CoGa, compare the highlighted regions in Fig. 9(c). Similarly, we can discuss the importance of covalent magnetism for the inverse structures. Comparing the spin-down DOS of conventional and inverse systems, the impression is that covalent magnetism helps to stabilize (FeCo)FeGa.

In order to gain further insight into systematic trends concerning the electronic properties of Heusler alloys we have plotted the total spin moments per formula unit as a function of the total number of valence electrons (Z) in Fig. 10 which shows an enlarged part of the original full Slater-Pauling curve for the 3d metals and binary alloys.[54] The reversal from increasing to decreasing inclination occurring in the results for $Fe_{3-x}Co_x$ can be correlated with the change observed when the majority-spin channel is completely occupied and the minority-spin channel becomes filled up. We compare our calculated spin moments for the Fe-Co-Ga-Zn systems (highlighted in red for the Ga-based and orange for the Zn-based compounds) with results for the half-metallic

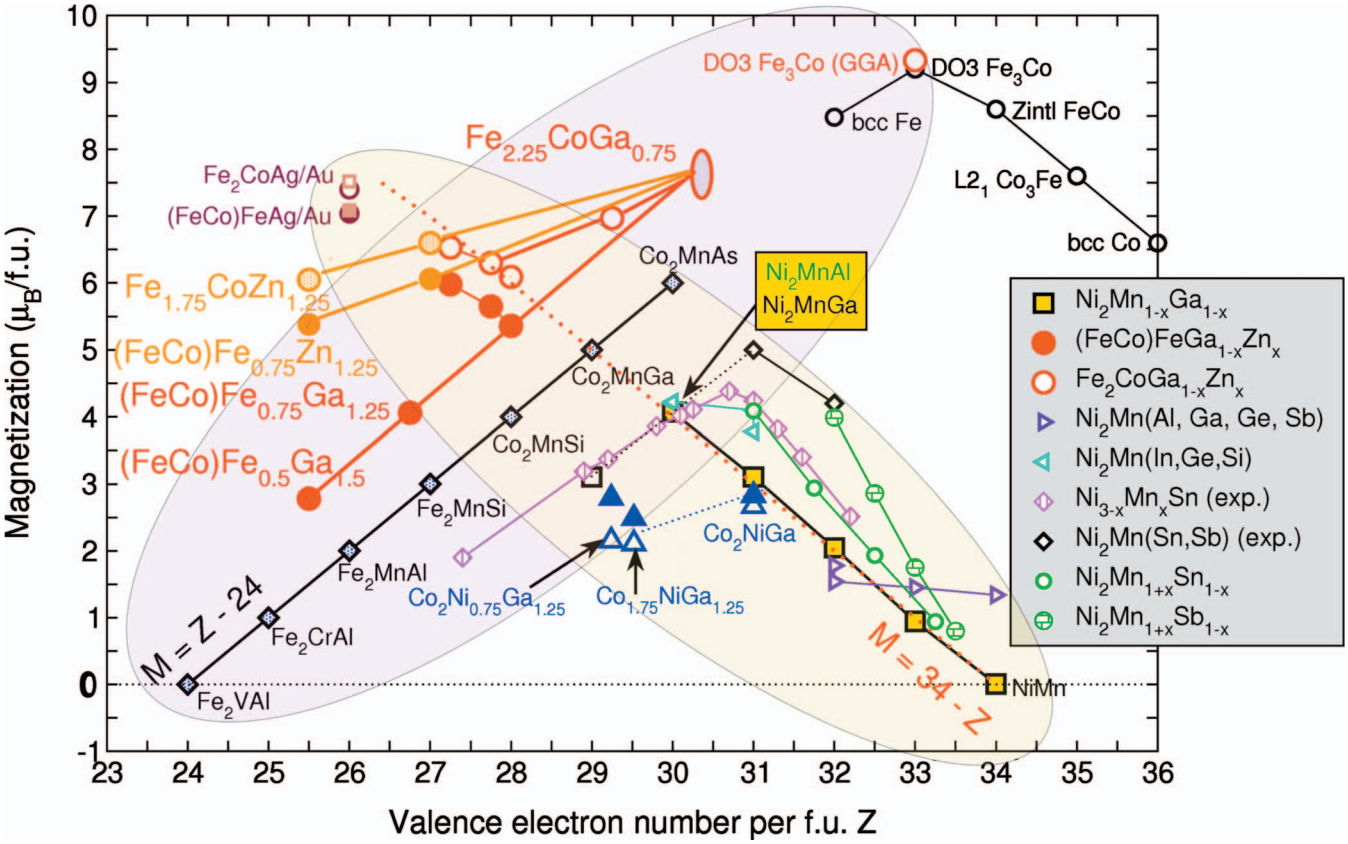

FIG. 10. (Color) Calculated spin moments per f.u. (highlighted in red for Ga-based and orange for Zn-based alloys) for the cubic conventional (open symbols) and the cubic inverse structures (filled symbols) as a function of the total number of valence electrons per f.u. Z in comparison to data found in literature. Please note that Z is always given for the Heusler structure, thus Z of Co in bcc structure is here $4\times9=36$. The half-metallic Heusler alloys (open, black diamonds) and our Fe-Co-Ga-Zn systems follow linear increasing functions indicating a fixed number of minority-spin states or reflecting an increasing percentage of Fe atoms in the compound, respectively. The linear decreasing slopes of the Ni-Mn-(Ga,Sn,Sb) systems originate from a constant number of majority spins or from increasing antiferromagnetic tendencies with increasing Mn concentration. The data of the stoichiometric $Fe_2Co(Ga,Zn)$ systems are perfectly in line with the results for Ni-Mn-Ga. This and the overall linear character of the spin moments imply that despite hybridization effects the magnetic moments possess localized character.

Heuslers found in literature[50] and other *ab initio* data for Ni-Mn-Z (Z=Ga,Al,In,Ge,Si),[47] Co-Ni-Ga, Ni-Co-Z (Z=Al,Ga,Ge,Sb),[47] and $Fe_{1-x}Co_x$.[18] The linear increasing function with increasing valence-electron number (Z), $M=Z-24$, of the half-metallic Heuslers originates from the filling of the majority-spin channel under a constant number of minority-spin states due to the pinning of the Fermi level in the half-metallic minority-spin gap. That the total moment follows this simple rule results from the fact that in total one has 12 occupied minority-spin states, one with s, three with p, and eight with d character. For details see the paper by Galanakis *et al.*[50] A linear decreasing slope, as found, e.g., for the Ni-Mn_{1+x}(Ga,In,Sn,Sb)$_{1-x}$ systems, hints toward a fixed number of majority spins (and corresponding filling of the minority-spin channel) or an increasing amount of antiferromagnetic tendencies with increasing Mn content in the Mn-based compounds, respectively. Our results meet the simple function $M=34-Z$ which hints toward 34 occupied majority-spin states per unit cell if we apply the hybridization picture drawn by Galanakis *et al.*

For the Fe-Co-based Heuslers we explain the increasing slope with an increasing percentage of ferromagnetic Fe replacing diamagnetic Ga in the compound. Extraordinarily high magnetic moments can be found for the Fe_2CoZ Heuslers (up to $M=7.5$ μ_B/f.u. for Fe_2CoAu) for which the Fe moment is significantly higher than in the elemental bcc bulk Fe phase. Variation in the Z element from Ga over Zn to Cu, Ag, and Au (decreasing Z) steadily enhances the total magnetic moment. Thus, one may suggest that in Z elements with an unfilled d shell the Z d electrons hybridize with the X d and Y d electrons and therefore the spin moments localized on Fe and Co atoms are enhanced. This scenario already starts with Zn as Z element showing that the hybridization of Zn s electrons with X d and Y d electrons leads to an emptying of the minority-spin channel as discussed in Sec. III F. Extrapolation of the linear increasing functions with slightly different slopes which are found for the inverse and conventional Fe_2CoGa and Fe_2CoZn systems coincide at a valence-electron number of approximately $Z=30.5$ which correspond to a composition of $Fe_{2.5}CoGa_{0.5}$. This nicely reflects the fact that a distinction in between inverse and conventional Heusler structure is no longer meaningful for the case that the cubic (Y, Z) sublattice of the Heusler structure is less than half occupied with the Z element.

The *ab initio* results for Ni-Mn-(Ga,Sn,Sb) obey linear functions with different slopes which emerge from the fact that all Ni-Mn-*Z* curves finally coincide at antiferromagnetic NiMn. Thus, *Z* element *sp*-electrons hybridize with *X d* and *Y d* electrons and cause a reduction in the total moment with increasing *Z* by filling of the minority-spin channel. The results for $Ni_2Co(Ga,Ge,Sb)$ seem to establish this observation as the spin moments slightly decrease with increasing *Z* as seen for $Ni_2Mn(Ga,Ge,Sb)$. Interestingly, the investigated stoichiometric Fe_2CoZ alloys are perfectly in line with the Ni-Mn-Ga results indicating that the depletion of the minority-spin channel with decreasing valence-electron number continues independent of the group of Heuslers considered.

In general, we find a set of linear increasing and linear decreasing functions which connect the magnetic spin moments of various families of Heusler alloys. This implies that despite hybridization effects the overall character of the magnetic moments in Heusler alloys is of localized nature.

H. Inverse martensites

The stability of the cubic inverse structures and the absence of a tetragonally distorted phase in $(FeCo)FeGa_{1-x}Zn_x$ systems make these systems inadequate for magnetic shape-memory purposes. So far, only few FSMAs are known which show a martensitic transformation in the inverse structure. But as (FeCo)FeZn already shows pronounced tendencies for a second-energy minimum at c/a ratios larger than one, we have done calculations for Fe-Co-based systems with slightly different composition or different *Z* components, in order to force these systems to undergo a martensitic instability (cf. Fig. 11). We succeeded by using rather unusual *Z* elements such as Cu, Ag, and Au (results for Fe_2CoAg or Fe_2CoAu are not shown because qualitatively the same behavior is found) or by a further enhancement of the Zn content in the Fe-Co-Zn compound ($Fe_{1.75}CoZn_{1.25}$). Remarkable is the occurrence of a local-energy minimum at $c/a<1$ as soon as an absolute energy minimum at $c/a>1$ could be induced. This is an important observation because the modulated phases which are relevant for the magnetic shape-memory effect are found at c/a ratios smaller than one.

Although all of these systems possess a positive mixing energy we believe that this study shows that it is possible to find an inverse martensite with high Curie and martensite transformation temperatures relevant for magnetic shape-memory purposes.

IV. CONCLUSION

The Curie temperatures of all investigated systems, Fe_2CoGa, $Fe_2CoGa_{0.75}Zn_{0.25}$, $Fe_2CoGa_{0.25}Zn_{0.75}$, and Fe_2CoZn, are remarkably high compared with prototype Ni_2MnGa FSMA (T_C=365 K). The successive substitution of Ga by Zn in the quaternary system $Fe_2CoGa_{1-x}Zn_x$ helps to reduce the energetic preference of the inverse cubic Heusler structure in favor of the tetragonally distorted conventional structure and increases T_C. However, this is achieved at the expense of structural stability. In $Fe_2CoZn_{0.75}Ga_{0.25}$ the

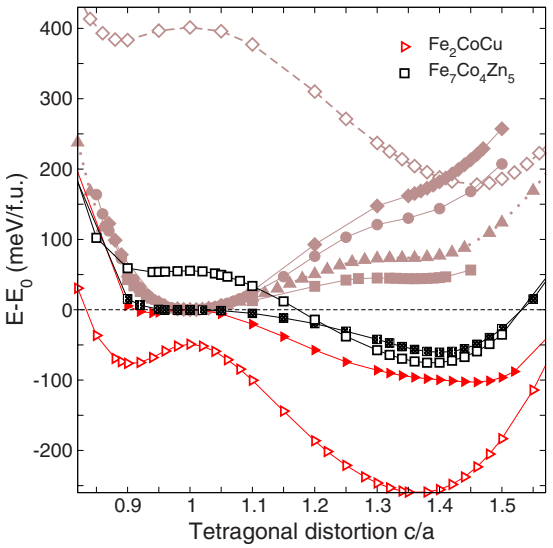

FIG. 11. (Color online) Total energy of a few previously unconsidered alloys relative to the energy of the respective cubic inverse phase. As in Fig. 2, open and filled symbols distinguish between conventional and inverse structures, respectively. For comparison the corresponding curves of all alloys discussed above in the inverse structure and of $L2_1$ Fe_2CoGa (from Fig. 2) are shown by gray symbols. In addition, results for two representative alloys, $Fe_7Co_4Zn_5$ (black squares) and Fe_2CoCu (red, rightward triangles) are also shown. For the latter two systems, clear martensitic tendencies are observed.

absolute energy minima of cubic inverse and conventional tetragonal Heusler structures are almost degenerate which would support coexisting inverse and conventional structures in disordered alloys. Therefore, we expect that $Fe_2CoZn_{1-x}Ga_x$ alloys are promising candidates which show the magnetic shape-memory effect.

This competition of conventional and inverse Heusler structures is rather intriguing. We have found that one important reason for the energetic preference of the inverse structures at $c/a=1$ with respect to the conventional structure at the same c/a in Ga-rich $Fe_2CoZn_{1-x}Ga_x$ alloys is the different atomic environment of Fe. In the inverse phase Fe_C is in a bcc-like atomic neighborhood with Fe_A and Co as nearest neighbors. In the unfavorable conventional phase, the hybridization of Fe and Co is partially suppressed by the different symmetries of Fe *d* and Co *d* orbitals (e_u, e_g and t_{1u}, t_{2g}) which results from the effect of different crystal fields acting on the octahedrally coordinated Fe and tetrahedrally coordinated Co. On the other hand, aspects of covalent magnetism give rise to enhanced hybridization effects in both spin channels of Fe_2CoGa as discussed above.

One important statement that emerges is that the *X* atoms which prefer a fcc close-packed crystal structure will stabilize the conventional X_2YZ Heusler structure as Ni in Ni_2MnGa or Co in Co_2FeGa. This is in contrast to *X* atoms with an elemental bcc-crystal structure which is responsible for the instability of the conventional structure and stabilizes the inverse Heusler structure like Fe in (FeCo)FeGa and in (FeCo)FeSi.

By the use of rather extraordinary *Z* elements such as Cu, Ag, or Au or by further enhancement of the Zn content we

could induce a martensitic instability also in the inverse Fe-Co-based Heuslers. Thus, although the latter alloys have a positive mixing energy we may tentatively conclude that it is possible to find exceptional FSMAs with high Curie temperature relevant for the magnetic shape-memory effect which show the martensitic transformation in the inverse structure.

With respect to magnetism, we compare the behavior of Fe_2CoGa and (FeCo)FeGa with the magnetic structure of another Heusler or Zintl phase, Fe_3Co or Fe_2FeCo, which also has two inequivalent Fe atoms and shows spin-dependent hybridization of Fe-Co *d* states (covalent magnetism).

Slater Pauling behavior could be established for all investigated Fe-Co-based Heusler alloys and is confirmed by other *ab initio* and experimental data found in literature. The linear increasing or decreasing slope of the spin moments of all Heusler alloys considered implies that despite hybridization effects the overall character of the magnetic moments is of localized nature.

ACKNOWLEDGMENTS

The authors would like to thank A. Hucht for helping with the Monte Carlo simulations and H. C. Herper for discussions. Antje Dannenberg, Markus E. Gruner, and Peter Entel acknowledge financial support by the Deutsche Forschungsgemeinschaft (SPP 1239).

[1] A. Sozinov, A. A. Likhachev, N. Lanska, and K. Ullakko, Appl. Phys. Lett. **80**, 1746 (2002).
[2] R. Kainuma, F. Gejima, Y. Sutou, I. Ohnuma, and K. Ishida, Mater. Trans., JIM **41**, 943 (2000).
[3] Y. Sutou, Y. Imano, N. Koeda, T. Omori, R. Kainuma, K. Ishida, and K. Oikawa, Appl. Phys. Lett. **85**, 4358 (2004).
[4] W. Maziarz, J. Dutkiewicz, R. Santamarta, and E. Cesari, Eur. Phys. J. Spec. Top. **158**, 137 (2008).
[5] Y. Tanaka, K. Oikawa, Y. Sutou, T. Omori, R. Kainuma, and K. Ishida, Mater. Sci. Eng. A **438-440**, 1054 (2006).
[6] P. J. Brown, K. Ishida, R. Kainuma, T. Kanomata, K. U. Neumann, K. Oikawa, B. Ouladdiaf, and K. R. A. Ziebeck, J. Phys.: Condens. Matter **17**, 1301 (2005).
[7] V. A. Chernenko, J. Pons, E. Cesari, and I. K. Zasimchuk, Scr. Mater. **50**, 225 (2004).
[8] K. Oikawa, T. Ots, F. Gejima, T. Ohmori, R. Kainuma, and K. Ishida, Mater. Trans. **42**, 2472 (2001).
[9] K. Oikawa, L. Wulff, T. Iijima, F. Gelima, T. Ohmori, A. Fujita, K. Fukamichi, R. Kainuma, and K. Ishida, Appl. Phys. Lett. **79**, 3290 (2001).
[10] M. Wuttig, J. Li, and C. Craciunescu, Scr. Mater. **44**, 2393 (2001).
[11] C. Craciunescu, Y. Kishi, A. T. Lograsso, and M. Wuttig, Scr. Mater. **47**, 285 (2002).
[12] K. Oikawa, T. Ota, Y. Tanaka, T. Omori, R. Kainuma, and K. Ishida, Trans. Mater. Res. Soc. Jpn. **28**, 265 (2003).
[13] N. Koeda, Y. Sutou, T. Omori, K. Oikawa, R. Kainuma, and K. Ishida, Scr. Mater. **52**, 1153 (2005).
[14] K. Oikawa, N. Koeda, Y. Sutou, T. Omori, R. Kainuma, and K. Ishida, Mater. Trans. **45**, 2780 (2004).
[15] Y. N. Zhang, J. X. Cao, and R. Q. Wu, Appl. Phys. Lett. **96**, 062508 (2010).
[16] R. Wu, J. Appl. Phys. **91**, 7358 (2002).
[17] J. R. Cullen, A. E. Clark, M. Wun-Fogle, J. B. Restor, and T. A. Lograsso, J. Magn. Magn. Mater. **226-230**, 948 (2001).
[18] K. Schwarz, P. Mohn, P. Blaha, and J. Kübler, J. Phys. F: Met. Phys. **14**, 2659 (1984).
[19] J. G. Booth and J. D. Marshall, Phys. Lett. **32**, 149 (1970).
[20] T. Takayama, S. Shinohara, K. Ishida, and T. Nishizawa, J. Phase Equilib. **16**, 390 (1995).
[21] A. J. Morton, Phys. Status Solidi A **44**, 205 (1977).
[22] R. Corson, S. Thuanboon, and S. Guruswamy, TMS Annual Meeting, 2006 (unpublished), p. 221.
[23] M. Ishimoto, H. Numakura, and M. Wuttig, Mater. Sci. Eng., A **442**, 195 (2006).
[24] Z. Lei, J. Cheng-Bao, S. Jia-Xiang, and X. Hui-Bin, Chin. Phys. B **18**, 1647 (2009).
[25] J. Van Humbeeck, J. Janssen, N. Mwamba, and L. Delaey, Scr. Metall. **18**, 893 (1984).
[26] J. Gil and J. M. Guilemany, J. Mater. Sci. Lett. **11**, 493 (1992).
[27] W. H. Zou, C. W. H. Lam, C. Y. Chung, and J. K. L. Lai, Metall. Mater. Trans. A **29**, 1865 (1998).
[28] A. Planes, L. Manosa, and M. Acet, J. Phys.: Condens. Matter **21**, 233201 (2010).
[29] P. Entel, M. E. Gruner, A. Dannenberg, M. Siewert, S. K. Nayak, H. C. Herper, and V. D. Buchelnikov, Mater. Sci. Forum **635**, 3 (2009).
[30] M. Gilleßen and R. Dronskowski, J. Comput. Chem. **31**, 612 (2010).
[31] M. Gilleßen and R. Dronskowski, J. Comput. Chem. **30**, 1290 (2009).
[32] N. K. Jaggi, K. R. P. M. Rao, A. K. Grover, L. C. Gupta, R. Vijayaraghavan, and L. D. Khoi, Hyperfine Interact. **4**, 402 (1978).
[33] G. Kresse and J. Furthmüller, Phys. Rev. B **54**, 11169 (1996).
[34] H. Ebert, in *Lecture Notes in Physics*, edited by H. Dreysse (Springer, Berlin, 2000), Vol. 50, p. 191.
[35] H. Ebert *et al.*, http://olymp.cup.uni-muenchen.de/ak/ebert/SPRKKR
[36] A. Ayuela, J. Enkovaara, K. Ullakko, and R. M. Nieminen, J. Phys.: Condens. Matter **11**, 2017 (1999).
[37] S. E. Kulkova, S. V. Eremeev, and S. S. Kulkov, Solid State Commun. **130**, 793 (2004).
[38] G. Kresse and D. Joubert, Phys. Rev. B **59**, 1758 (1999).
[39] J. P. Perdew, K. Burke, and M. Ernzerhof, Phys. Rev. Lett. **77**, 3865 (1996).
[40] J. P. Perdew, J. A. Chevary, S. H. Vosko, K. A. Jackson, M. R. Pederson, D. J. Singh, and C. Fiolhais, Phys. Rev. B **46**, 6671 (1992).
[41] S. E. Kulkova, S. S. Kulkov, and A. V. Subashiev, Comput.

Mater. Sci. **36**, 249 (2006).
[42] E. C. Bain, Trans. AIME **70**, 25 (1924).
[43] C. M. Wayman, Mater. Sci. Forum **56-58**, 1 (1990).
[44] A. R. Williams, V. L. Moruzzi, J. C. D. Gelatt, J. Kübler, and K. Schwarz, J. Appl. Phys. **53**, 2019 (1982).
[45] V. Crisan, H. Ebert, P. Entel, and H. Akai, Comput. Mater. Sci. **17**, 151 (2000).
[46] D. Alfè, Comput. Phys. Commun. **180**, 2622 (2009).
[47] A. T. Zayak, W. A. Adeagbo, P. Entel, and K. M. Rabe, Appl. Phys. Lett. **88**, 111903 (2006).
[48] R. Dronskowski and P. E. Blöchel, J. Phys. Chem. **97**, 8617 (1993).
[49] A. Ayuela, J. Enkovaara, K. Ullakko, and R. M. Nieminen, J. Phys.: Condens. Matter **14**, 5325 (2002).
[50] I. Galanakis, P. H. Dederichs, and N. Papanikolaou, Phys. Rev. B **66**, 174429 (2002).
[51] H. C. Herper (unpublished).
[52] M. E. Gruner (unpublished).
[53] M. Siewert, M. E. Gruner, A. Dannenberg, A. Hucht, S. M. Shapiro, G. Xu, D. L. Schlagel, T. A. Lograsso, and P. Entel, Phys. Rev. B **82**, 064420 (2010).
[54] A. Planes, L. Mañosa, and M. Acet, J. Phys. Chem. **21**, 233201 (2009).